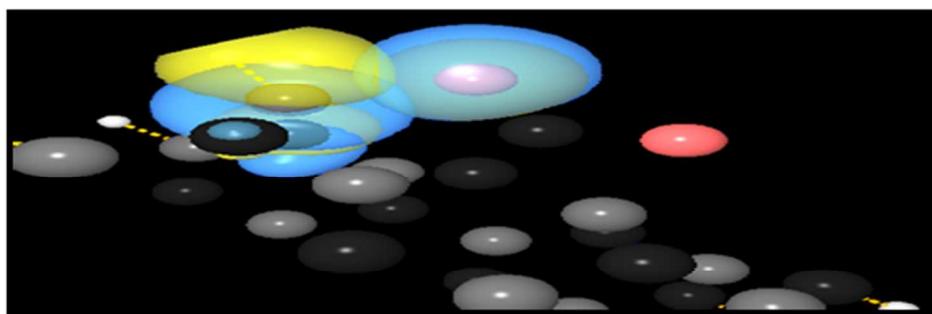




**Investigation of adsorption properties of the CS<sub>2</sub> on interior and exterior surfaces of single-walled silicon-carbide nanotube and effect of applied electric field: Electronic structure, charge density and NMR studies**

Journal:	<i>RSC Advances</i>
Manuscript ID	RA-ART-04-2015-006459.R2
Article Type:	Paper
Date Submitted by the Author:	02-Sep-2015
Complete List of Authors:	Ghiassi, Hamideh; University of Birjand, Chemistry Department Raissi, Heidar; University of Birjand, Chemistry
Subject area & keyword:	



The adsorption behavior of CS<sub>2</sub> on silicon-carbide nanotube has been investigated using B3LYP/6-31G\*. 3D NBO contour plots illustrating the interaction between lone pair orbitals of S atom of CS<sub>2</sub> with  $\sigma^*$ Si12-C13 of the nanotube in configuration 2

168x94mm (96 x 96 DPI)

# Investigation of adsorption properties of the CS<sub>2</sub> on interior and exterior surfaces of single-walled silicon-carbide nanotube and effect of applied electric field: Electronic structure, charge density and NMR studies

Hamideh Ghiassi\* and Heidar Raissi

Chemistry Department, University of Birjand, Birjand, Iran

## ABSTRACT

The adsorption behavior of the CS<sub>2</sub> on the surface of silicon-carbide nanotube (SiCNT) is studied by the Density Functional Theory. For both the external and internal cases, different configurations of the adsorbed CS<sub>2</sub> onto the nanotube surface are studied. The energetic, geometric, and electronic properties have been investigated using B3LYP density functional. According to the obtained results, the process of CS<sub>2</sub> molecule adsorption on different sites of the out wall of the nanotube is exothermic and configurations are stable, while the process of CS<sub>2</sub> molecule adsorption on the internal surface of the SiCNT is endothermic. The adsorption energy values indicated that the CS<sub>2</sub> molecule can be physically or chemically adsorbed on the external surface of the SiCNT while for internal case, it can be chemically adsorbed on the internal wall. NBO analysis indicated that the CS<sub>2</sub> molecule can be adsorbed on the nanotube with a charge transfer from CS<sub>2</sub> molecule to nanotube. <sup>13</sup>C and <sup>29</sup>Si chemical shielding tensors are computed using GIAO method. NMR calculations reveal that <sup>13</sup>C and <sup>29</sup>Si chemical shielding is changed upon the CS<sub>2</sub> adsorption. As well as, the effect of external electric fields (EFs) on the adsorption properties of the geometric structures, adsorption energies, band gap has been considered.

**Keywords:** Adsorption, SiCNT, CS<sub>2</sub>, Adsorption energy, NMR, AIM, NBO

---

\* Corresponding author. Tel.: +985612502064; fax: +985612502065.  
E-mail address: hamidehghiassi@birjand.ac.ir (H.Ghiassi).

## 1. INTRODUCTION

Carbon disulfide ( $\text{CS}_2$ ) is a clear, colourless or faintly yellow, mobile liquid at room temperature. It is also produced naturally by soil and sediment microorganisms, vegetation, forest and grass fires, and volcanoes. Carbon disulfide is ubiquitous throughout the environment. It has been detected in air, water, sediment, and soil; however, it is present primarily in the air. Carbon disulfide is not only extensively used in industry and laboratories as solvent or a reactive reagent but also frequently used for dry cleaning and as an insecticide for the conservation of grains. Longtime exposure to even low concentrations of  $\text{CS}_2$  can also cause various health risks. It has been considered to be one of the most toxic substances lead to damage to the blood vessels of the retina, nervous system diseases [1], coronary artery diseases and (with higher exposures) increased mortality from heart disease. Therefore, the American Conference of Government Industrial Hygienists has controlled the level of  $\text{CS}_2$  in the air.

Controlling the  $\text{CS}_2$  concentration under the threshold limit value in the air requires a sensitive, reliable, and specific method for monitoring its content in work environments. Due to detect  $\text{CS}_2$  concentration in the air, Gas sensors have been considered promising alternatives for environmental measurements due to their low cost, high sensitivity, fast response and direct electronic interface [2,3]. In recent years, Nanotubes have attracted great interest in the sensor industry. Carbon nanotubes (CNTs) as chemical sensors [4-8] have generated strong interests in the research community since Kong et al. [4,5] demonstrated that single-walled carbon nanotubes (SWCNT) can be used as miniature sensors to detect low concentrations of toxic gas molecules. Silicon carbide nanotubes (SiCNTs) have some advantages over CNTs, due to its unique properties [9–19], including good chemical reactivity and high stability at high temperatures, high power, and in harsh environments. Therefore, they may possess high reactivity of exterior surface facilitating to sidewall decoration and stability at high-temperature. The SiCNT might have great potential applications in many areas including gas sensors [20, 21], hydrogen storages [22], metal-free catalysts [23], and special (nano) optical devices [24, 25].

We studied the  $\text{CS}_2$  adsorption onto the interior and exterior surfaces of SiCNT using density functional theory (DFT), with the aim of understanding the adsorption behavior at various sites. In order to find the preferred absorption site, different positions are considered. The effects of adsorption on the structural and electronic properties of SiCNT are investigated.

## 2. Computational Methods

In this work, we investigated the adsorption behavior of the CS<sub>2</sub> molecule over the all active sites of the zigzag single wall (6, 0) SiCNT, in which the end atoms have been saturated with hydrogen atoms to avoid the boundary effects. Selected nanotube includes 24 pairs Si and C atoms.

DFT and DFT-D methods [26] is used to study the structural and electronic properties of the adsorption configurations of CS<sub>2</sub> molecule. In all cases, the computations are carried out with the B3LYP/6-31G\*[27], B3LYP-D and CAM-B3LYP levels of theory. CAM-B3LYP is a long-range corrected version of B3LYP which includes exact Hartree-Fock exchange at long distances [28]. In DFT-D approach as developed by Grimme [29], the dispersion corrected total energy is given by

$$E_{\text{DFT-D}} = E_{\text{KS-DFT}} + E_{\text{disp}} \quad (1)$$

Where  $E_{\text{KS-DFT}}$  is the usual self-consistent kohn-sham energy as obtained from the chosen density functional and  $E_{\text{disp}}$  is an empirical dispersion correction.

The population analysis, the electronic- contour plot for the highest occupied molecular orbital (HOMO) and the lowest unoccupied molecular orbital (LUMO), calculation of HOMO-LUMO energy gap ( $E_g$ ) and density of states (DOS) are used for studying the electronic properties of nanotube. Vibrational frequencies are computed at the same level of theory to check whether stationary points are corresponding to true minima on the potential energy surface. The adsorption energy between CS<sub>2</sub> molecule and nanotube is corrected using the counterpoise technique proposed by Boys and Bernardi [30] and zero point vibrational energy (ZPVE) correction. The adsorption energy is estimated using the following approximate expression:

$$E_{\text{ads}} = E_{\text{CS}_2/\text{SiCNT}} - (E_{\text{SiCNT}} + E_{\text{CS}_2}) \quad (2)$$

Where  $E(\text{CS}_2/\text{SiCNT})$  corresponds to the energy of the SiCNT in which the CS<sub>2</sub> molecule have been adsorbed on the wall,  $E(\text{SiCNT})$  is the energy of the isolated nanotube, and  $E(\text{CS}_2)$  is the energy of a single CS<sub>2</sub> molecule. It should be mentioned that the adsorption energy is the sum of interaction and deformation energy. The following equations are applied to calculate these contributions

$$E_{\text{ads}} = E_{\text{def}} + E_{\text{int}} \quad (3)$$

$$E_{\text{int}} = E_{\text{tube-gas}} - (E_{\text{tube in complex}} + E_{\text{gas in complex}}) \quad (4)$$

$$E_{\text{def}} = E_{\text{def gas}} + E_{\text{def tube}} \quad (5)$$

Where  $E_{\text{tube in complex}}/E_{\text{gas in the complex}}$  are the total energy of nanotube/gas and  $E_{\text{def tube}}/E_{\text{def gas}}$  are the deformation energy of nanotube/gas in its optimized geometry.

The molecular orbital (MO) calculations such as HOMO-LUMO are performed on selected configurations. Conceptual density functional theory provides insights into the popular qualitative chemical concepts such as electronic chemical potential ( $\mu$ ) [31], hardness ( $\eta$ ) [32, 33] and electronegativity ( $\chi$ ).  $\chi$  is defined as the negative of  $\mu$  ( $\chi = -\mu$ ). We calculate the chemical potential ( $\mu$ ) and global hardness ( $\eta$ ) of the complexes, as given below:

$$\eta = (E_{\text{LUMO}} - E_{\text{HOMO}})/2, \quad \mu = (E_{\text{LUMO}} + E_{\text{HOMO}})/2 \quad (6)$$

Where  $E_{\text{HOMO}}$  is the energy of the highest occupied molecular orbital and  $E_{\text{LUMO}}$  is the energy of the lowest unoccupied molecular orbital.

Delocalization of electron density between the filled Lewis type NBOs (Natural Bond Orbital) and empty antibonding non-Lewis NBOs is calculated by NBO analyzing [34, 35] as implemented in the Gaussian 03 package [36]. The contour plot for visualization of the NBO result is constructed by the NBOView software [37] package using the standard keywords implemented therein.

The analysis of the distribution of electron densities is performed to find the bond critical points and to characterize them in terms of values of electron densities ( $\rho$ ) and their Laplacian ( $\nabla^2\rho$ ). The AIM calculations [38] are carried out using the AIM2000 program [39].

The chemical shielding tensors (CS) at the sites of C and Si nuclei are calculated using the Gauge-Independent Atomic Orbital (GIAO) method [40]. The quantum chemical calculations yield chemical shielding tensors in the principal axis system (PAS) with the order of  $\sigma_{33} > \sigma_{22} > \sigma_{11}$ ; therefore, Eqs. (7) and (8) are used to convert the calculated chemical shielding tensors to the absolute isotropic ( $\sigma_{\text{iso}}$ ) and anisotropic ( $\Delta\sigma$ ) chemical shielding parameters:

$$\sigma_{\text{iso}} = (\sigma_{33} + \sigma_{22} + \sigma_{11})/3 \quad (7)$$

$$\Delta\sigma = \sigma_{33} - (\sigma_{11} + \sigma_{22})/2 \quad (8)$$

Wiberg bond index (WBI) [41, 42] relates to the bond order and demonstrates the strength of the covalent character. It expressed by the following mathematical definition:

$$\text{WBI} = \sum_k P_{jk}^2 = 2P_{jj} - P_{jj}^2 \quad (9)$$

Where  $p_{jk}$  and  $p_{ij}$  denote the density matrix elements and charge density in the atomic orbital, respectively.

The work function ( $\Phi$ ) is the minimum energy required to extract one electron from the Fermi level to the vacuum. It can be estimated as the difference between vacuum level and Fermi level, which herein, the energy of vacuum level has been assumed to be zero. The canonical assumption for Fermi level is that in a molecule (at  $T = 0\text{K}$ ) it lies approximately in the middle of the Eg. As well as, the numerical values of the applied uniform external electric field are 0.0025, 0.005 a.u. ( $1 \text{ a.u.} = 5.14224 \times 10^{11} \text{ V/m}$ ) along perpendicular and parallel directions to the axis of the tube.

Ab-initio calculations based on the generalized gradient approximation (GGA) with the PW91 exchange-correlation functional [44] in density functional theory are performed using Quantum Espresso and The pseudopotential plane wave calculations have been performed using ultrasoft pseudopotentials. The supercell is (6, 0) SiCNT, that consisted of 24 pairs Si and C atoms in tetragonal structure with parameters  $a=b=23 \text{ \AA}$ ,  $c=10.8 \text{ \AA}$ . For the current calculations, the energy cutoff of the plane wave basis set is set high enough (40 Ry) to ensure accurate results. The force on each ion is converged to be less than  $10^{-4} \text{ Ry/Bohr}$ , and all the geometric structures are fully relaxed to minimize the total energy of the system until a precision of  $10^{-7} \text{ Ry}$  is reached. Along the tube axis,  $1 \times 1 \times 7$  Monkhorst–Pack k-points are used for the Brillouin zone integration. DFT calculations on the band structures and density of states (DOS) using denser  $1 \times 1 \times 20$  special k-points are performed.

### 3. Results and Discussion

#### 3.1. Molecular geometry and Binding energies

in order to determine the most stable configuration, different configurations of  $\text{CS}_2$  molecule adsorbed on the out wall of the nanotube and two cases for their adsorption on the inside of the nanotube ( $\text{CS}_2$  perpendicular and parallel to the z axis of the tubes) have been considered. Several of distinct starting structures have been considered for optimization. After structural optimizations, re-orientation of the molecule has been predicted in some configurations, and finally stable configurations are obtained. The initial and final optimized geometry of the  $\text{CS}_2/\text{SiCNT}$  complexes and SiCNT is depicted in Figures 1,2 and 3.

Table 1 illustrates the geometrical parameters and the interaction ( $E_{\text{int}}$ ), deformation ( $E_{\text{def}}$ ) and adsorption ( $E_{\text{ads}}$ ) energies for the studied complexes. Our results indicated that the SiCNT has two types of Si-C bonds, one with a bond length of  $1.839 \text{ \AA}$  and parallel with the nanotube axis, and another with a bond length of  $1.777 \text{ \AA}$ , but not in parallel with the nanotube axis. Our results indicated that optimized parameters of the B3LYP-D are almost the same as the ones of B3LYP. In other words, the dispersion term does not contribute to the geometry of the pristine SiCNT. As well as, calculations are performed with Quantum espresso indicate that the SiCNT has two types of Si-C bonds. The lengths of C-Si bonds are about  $1.79 \text{ \AA}$  and  $1.80 \text{ \AA}$  for axial and circumferential, respectively. As the atomic radius of Si is larger than that of a C atom, the wall surface of the SiCNT is rugged and Si atoms slightly protrude out of the surface. The charge analysis indicate that electrons are transferred from the silicon atom to the vicinity of the carbon atoms, indicating that the C-Si bonds of the sidewall are partially ionic. This results is agreement with results of Gaussian. As well as, calculations are performed for the configuration 2 with this software. Our results indicate that upon  $\text{CS}_2$  adsorption on the SiCNT surface, the C-Si bonds length in the region of  $\text{CS}_2$  molecule adsorption are longer than that in the pristine nanotube and the equilibrium distances of the S-Si and  $\text{C}_{\text{CS}_2}\text{-C}_{\text{Nanotube}}$  are about  $2.987$  and  $3.667 \text{ \AA}$ , respectively and adsorption energy is about  $-0.14\text{eV}$ .

Inspection of theoretical results indicates that  $E_{\text{ad}}$  for the studied complexes varies from  $-163.99$  to  $885.39 \text{ KJ/mol}$ . These values indicate that the  $\text{CS}_2$  molecule can be physically or chemically adsorbed on the surface of the SiCNT. The most stable configuration is configuration 2 (see Fig. 2) which in this configuration, the atoms of sulfur and carbon of the  $\text{CS}_2$  molecule prefer to attach to silicon and carbon atoms of the nanotube by distances of  $2.423$  and  $1.486 \text{ \AA}$ , respectively. Our theoretical results indicate that a structural deformation to both the  $\text{CS}_2$  molecule and SiCNT is observed by adsorption of the  $\text{CS}_2$  molecule on the SiCNT nanotube in the most stable configuration. The adsorbed  $\text{CS}_2$  causes the Si6-C1 bond to be pulled inward from the nanotube wall with the bond length increasing from  $1.778$  of the free nanotube to  $1.906 \text{ \AA}$  in the  $\text{CS}_2$  adsorbed form because the chemisorption of  $\text{CS}_2$  on the SiCNT causes the  $\text{SP}^2$  hybridization of the C1-Si6 bond in the nanotube wall change to the  $\text{SP}^3$  hybridization and hence the Si6-C1 bond length increases. It is worth mentioning that the  $\text{CS}_2$  structure changes upon adsorption on SiCNT. As known isolated  $\text{CS}_2$  molecule is a totally planar molecule with S-C-S angle of  $180$ . When the  $\text{CS}_2$  is adsorbed on the SiCNT, significant out-of-plane displacement of

the S atoms is observed. Therefore, the S-C-S angle in this configuration is reduced to  $125.2^\circ$ . In addition, the C17-S19 bond length in this configuration is about  $1.738 \text{ \AA}$ , which is longer than that in the free molecule. The calculated  $E_{\text{ad}}$  value is about  $-163.98 \text{ KJ/mol}$  ( $-1.702 \text{ eV/mol}$ ) for the most stable configuration, which implies to the chemisorption process. The negative  $E_{\text{ad}}$  value indicates that this process energetically is favorable and exothermic. In order to examine the deformation degree of the nanotube after  $\text{CS}_2$  molecule attached to the nanotube, deformation energy is calculated. As it is stated, the adsorption energy is the sum of two components, interaction and deformation energy. Inspection of Table 1 reveals clearly that the deformation energy of the studied complexes is in range of  $-34$ - $723 \text{ KJ/mol}$ . The obtained deformation energy value for the most stable configuration is  $341.03 \text{ KJ/mol}$  ( $3.540 \text{ eV/mol}$ ). On the other hand, the value of the interaction energy for this configuration is  $-505.19 \text{ KJ/mol}$  ( $-5.245 \text{ eV/mol}$ ), which indicates that  $\text{CS}_2$  molecule can be chemisorbed onto the nanotube surface by the formation of new chemical bond between  $\text{CS}_2$  molecule and nanotube surface. Calculated vibrational frequency of C17-S19 in this configuration is smaller than that in the free molecule, indicating that the length of the C17-S19 bond should be increased upon the adsorption process.

Physisorption is the other type of the interaction between  $\text{CS}_2$  and nanotube that this type adsorption takes place in the configurations 1, 3, 4, 6, 7, 8. In the configuration 1,  $\text{CS}_2$  molecule puts a top of a C1 atom by a distance of  $3.887 \text{ \AA}$ . The value of the adsorption energy for this configuration is about  $-40.29 \text{ KJ/mol}$  ( $-0.418 \text{ eV/mol}$ ) that exhibiting a physisorption characteristic. Analysis of the structural parameters indicates that the C=S and C-Si bonds length are remained nearly constant. These results indicate that this interaction is weak. Here, it should be noted that the stretching mode of C=S in the configuration 1 occurs at slightly lower frequencies compared to that of the free molecule. Furthermore, the interaction energy for this configuration is about  $-5.91 \text{ KJ/mol}$ . Therefore, it can be concluded that this interaction is from of weak type. Also, the value of the deformation energy ( $-34.38 \text{ kJ/mol}$  ( $-0.357 \text{ eV/mol}$ )) confirms the less deformation degree in this configuration as compared to other configurations.

Our results indicate that the binding energies between the  $\text{CS}_2$  and nanotube are dependent on locations of the  $\text{CS}_2$ . Our theoretical results confirm that as the interaction becomes stronger, the deformation degree of the nanotube after absorbing the  $\text{CS}_2$  molecule becomes more. The maximum and minimum values of the deformation energy correspond to the configurations 9 and 1, respectively.

It can be seen that the adsorption energy of the CS<sub>2</sub> molecule on the internal surface is positive. This implies that the addition reaction is endothermic and the formed complexes are unstable. The obtained energy values reveal that the CS<sub>2</sub> molecule is chemically adsorbed on the internal wall of SiCNT. Moreover, after CS<sub>2</sub> adsorption on the internal surface of nanotube, a structural deformation to both the CS<sub>2</sub> molecule and nanotube is observed in configuration 9 (see Fig. 3). The obtained deformation and interaction energies for configuration 9 (723.79 and 161.61KJ/mol, respectively) indicate that the CS<sub>2</sub> molecule could be chemisorbed onto the internal surface of SiCNT.

For the most configurations, the DFT-D optimized structures show a decrease in the distance between nanotube and CS<sub>2</sub>, pulling the CS<sub>2</sub> closer to the nanotube surface. As well as, the use of the B3LYP-D results in noticeable change in the trends of adsorption energy. For investigated configurations, adding the dispersive interactions gives more endothermic adsorption. (see Table S1)

The geometry of the SiCNT and the complexes are optimized at the CAM-B3LYP/6-31G\*Level (see Table S2). In this approach, the adsorption energy varies from -172.89 to 890.62 KJ/mol. Further while improving the level of correlation treatment will decrease the adsorption energy value for some configurations. The calculated E<sub>ad</sub> value is about -172.853 KJ/mol for the most stable configuration.

### 3.2. Atoms-In-Molecules (AIM) analysis

In order to obtain the deeper insight into the nature and strength of the nanotube-molecule interaction in systems considered in this study, the analysis of electron density has been carried out. The  $\rho_{BCP}$ ,  $\nabla^2 \rho_{BCP}$  and the  $G_{BCP}$ ,  $V_{BCP}$  and  $H_{BCP}$  energy component values for all of the models examined in this work are collected in Table 2.

The results of topological analysis indicate that bonds along the nanotube circumference axis have a more electronic density than those of the parallel bonds with the nanotube axis. This is in agreement with the C-Si bond length of the nanotube as was discussed earlier in the previous section.

Analysis of topological parameters of the studied configurations given in Table 2 reveals that the BCPs corresponding to the C... X (X = C or Si atom of the nanotube) contact have negative  $\nabla^2 \rho_{BCP}$  and  $H_{BCP}$  values in the configurations 2, 5, 9 ( $\rho$  and  $\nabla^2$  (values vary from 0.17 a.u to

0.26 a.u. and from -0.58 a.u. to -0.2 a.u., respectively). A negative value of Laplacian exhibits concentrated accumulation of the electron density and it indicates a covalent bond. While  $\nabla^2\rho_{\text{BCP}}$  of the Y...X (Y=C or Si molecule, X=C or Si atoms of nanotube) contact is positive in the configurations 1, 4, 7, 8. ( $\rho$  and  $\nabla^2\rho$  values vary from 0.00295 a.u. to 0.00339 a.u. and from 0.00828 a.u. to 0.00984 a.u., respectively). These values indicating that the interaction in the mentioned systems may be classified as electrostatic interactions.

Inspection of topological parameters indicates in the most stable configuration, in comparison to free molecule, the electron density at the BCP of C=S bonds decreases. This result supported by the increase in the C=S bond length. It can be seen from Table 2 that the C1-Si2 electron density is reduced from 0.121 to 0.103 a.u. after adsorption process, which is consistent with elongation of the C1-Si2 bond length.

The contour map of the electron density for the most stable configuration is shown in Fig. 4. The obvious overlap of electron densities between C atom of the CS<sub>2</sub> molecule and C1 atom of the SiCNT indicates a covalent bonding between them that this observation is agreement with the topological parameters.

Our results indicate that the electron density of the C1-Si2 bond in the configuration 1 is constant after adsorption of the CS<sub>2</sub> molecule. This behavior can be explained by weakness of the interaction between SiCNT and CS<sub>2</sub> molecule. The contour map of the electron density for the configuration 1 shows that the electron density distribution between CS<sub>2</sub> molecule and nanotube is weak (see Fig. 4). This is agreement with the calculated adsorption energy.

Analysis of the electron density for the studied complexes indicate that the electron density at the BCP of nanotube...CS<sub>2</sub> contact becomes more as the interaction energy becomes larger.

Inspection of Table 2 emphasizes that the electron density of nanotube-CS<sub>2</sub> contact in the configuration 2 is more than that of the other configurations. This can be explained by stronger interaction in this configuration.

Investigation of the theoretical results reveals that there is a good correlation between  $\rho_{\text{nanotube...CS}_2}$  versus the nanotube...CS<sub>2</sub> bond length, for configurations which in the CS<sub>2</sub> is adsorbed on the outer surface of the nanotube, with a correlation coefficient about 0.9 and linear regression is given by equation presented below:

$$Y = -0.0797 x + 0.309 \quad (10)$$

Where  $Y$  corresponds to  $\rho_{\text{nanotube...CS}_2}$  and  $x$  corresponds to the nanotube...CS<sub>2</sub> bond length. These imply that the nanotube...CS<sub>2</sub> bond length can be very useful to estimate the  $\rho_{\text{nanotube...CS}_2}$ .

Deformation density map for the configuration 2 display in Fig.5 show SP<sup>2</sup> hybridization of the C1-Si6 bond in the nanotube wall change to the SP<sup>3</sup> hybridization and formation of the strong binding between C of the nanotube and C of the CS<sub>2</sub>.

### 3.3. Natural Bond Orbital analyses (NBO):

The NBO analysis is employed to study the intermolecular orbital interaction in the complexes. The results of our NBO analysis for studied configurations are provided in Table 3.

Analysis of NBO indicates that by adsorption of the CS<sub>2</sub> molecule on the nanotube surface in the most stable configuration, the s-character of the C atom in the C17=S19 bond of the CS<sub>2</sub> molecule is changed from 49.89% to 31.75 %, which indicate that the SP hybridization of the C atom in the CS<sub>2</sub> molecule is changed to nearly SP<sup>2</sup> hybridization in the adsorbed form on the SiCNT. These results are supported by the decrease of the S-C-S angle of CS<sub>2</sub> molecule.

The influence of CS<sub>2</sub>-SiCNT interaction on the bond order has investigated in this work. The smaller WBI implies to weaker covalent character. The analysis of WBI illustrates that in the most stable configuration, the adsorption of CS<sub>2</sub> on the outer surface of the SiCNT leads to decrease in the WBI of C1-Si2 and C17-S18 from 0.7877 to 0.5489 and from 1.9848 to 1.4709, respectively. These results are in agreement with obtained structural parameters for this configuration. On the other hand, for the configuration 1, the WBI of C1-Si2 bond is not considerably changed after CS<sub>2</sub> adsorption, indicating the CS<sub>2</sub> molecule adsorbs through weak interaction.

According to NBO analysis, the second-order perturbation stabilization energy  $E^{(2)}$  for the all configurations are computed and presented at the Table 3. The results of NBO analysis illustrate that in the most stable configuration, LP<sub>S19</sub>(lone pair) participates as donor and  $\sigma^*_{\text{C1-C17}}$  behaves as acceptor in strong intermolecular charge transfer interactions with the energy value of 4.48 kcal/mol. Thus the CS<sub>2</sub> acts as an electron donor.

Natural bond orbital analysis indicates that for the configuration 1 when the CS<sub>2</sub> molecule bonded to the SiCNT surface, the WBI of C-S bonds is remained nearly constant (1.9840), indicating the CS<sub>2</sub> molecule adsorbs through weak interaction.

It can be seen from Table 3,  $E^{(2)}$  value for the different configurations varies from 0.09 to 168 Kcal/mol. Inspection of the results reveals that there is a stronger interaction in the configuration 2 in comparison with configuration 1 because of more total charge transfer energy associated with the intermolecular interaction. The maximum and minimum values of  $E^{(2)}$  correspond to the configurations 9, 7, respectively. Fig. 6 shows 3D NBO contour plot illustrating the interaction between lone pair orbitals of S atom of  $CS_2$  with  $\sigma^*Si12-C13$  of the nanotube in configuration 2. Isosurface maps for the configurations 1, 2 are shown in Fig. 7. This figure shows that in the configuration 1,  $CS_2$  adsorbs physically, which is far from the nanotube surface, therefore has almost no effect on the electronic charge distribution of Si, C of the SiCNT; thus, no significant charge transfer occurs between the molecule and the nanotube. While, in the case of the configuration 2, strong hybridization of the C atom of the  $CS_2$  with the nanotube takes place, resulting in a significant charge transfer in the system.

### 3.4. Thermodynamic parameters

The calculated thermodynamic properties of the investigated systems are listed in Table 4. The complexes with lower relative standard Gibbs energy of formation are relatively more stable, whereas those with the higher relatively standard energy of formation are more unstable. The negative standard enthalpy change demonstrates that the formation of complexes is enthalpically favored. The values of the  $T\Delta S_{298}^0$  imply the large entropy changes during the formation of complexes. In the investigated complexes, the negative values of the  $T\Delta S_{298}^0$  and  $\Delta H_{298}^0$  determine the negative values of  $\Delta G_{298}^0$ . Thus, the formation of complexes is thermodynamically favored ( $\Delta G_{298}^0$ ).

### 3.5. HOMO and LUMO analysis

Fig. 8 shows LUMO and HOMO profiles of the  $CS_2$  molecule, SiCNT and configuration 2. It can be seen that the HOMO of  $CS_2$  molecule is positioned on the sulfur atoms and LUMO is located on the sulfur and carbon atoms.

Isosurface plots for HOMO and LUMO levels of (6,0) SiCNT show that the HOMO is positioned at the nanotube end, with most contributions at C atoms that are terminated by H atoms. In contrast, the LUMO is presented as  $\pi$  states localized at the Si-C pair along the nanotube axis. Therefore, it is expected that the  $CS_2$  molecule interacts with all atoms of

nanotube except for the end C atoms. The molecular orbital plots of configuration 2 indicate that after CS<sub>2</sub> adsorption, the LUMO is more localized on the nanotube and the HOMO is placed over the CS<sub>2</sub>, indicating that electrons transfer from CS<sub>2</sub> molecule to SiCNT.

Inspection of our theoretical results reveals that after absorbing the CS<sub>2</sub> molecule on the surface of nanotube, for configurations 2, 3, 5 and 6, the hardness value of the complexes is slightly reduced and their reactivities are increased.

It can be seen from Table 4, upon CS<sub>2</sub> adsorption, the Eg slightly decreases for above configurations, thus the electric conductivity of the SiCNT will not considerably change in the presence of CS<sub>2</sub> which can be explained according to the following equation

$$\sigma \propto \exp(-E_g/2KT)$$

Where  $\sigma$  is the electrical conductivity and K is the Boltzmann's constant. According to this equation, smaller Eg values lead to the higher conductance at a given temperature.

Our theoretical results indicate that the amount of Eg in configurations 1, 4, 7, 8, 9 and 10 is higher than the pristine form. Higher Eg values of the nanotubes after CS<sub>2</sub> adsorption confirm their relative stability of kinetic in comparison to the pristine form. Therefore, it is energetically unfavorable to add electrons to a high-lying LUMO, and to extract electrons from a low-lying HOMO. The maximum and minimum values of Eg correspond to the configurations 10 and 2, respectively. It is worth mentioning that the Eg values for configurations in which CS<sub>2</sub> absorbed on the exterior surface of nanotube are lower than the configurations which CS<sub>2</sub> absorbed on the interior surface of nanotube.

In the configuration 2, when the CS<sub>2</sub> molecule approaches the SiCNT surface, electronic interaction among nuclei and electrons disturb the initial configuration, inducing adsorption of the CS<sub>2</sub> on the nanotube surface and charge transfers to nanotube, making nanotube electronegative and forming an additional electric field. Reconstruction induces a decrease of Eg [45].

The calculations of the density of state (DOS) for the pristine SiCNT and configuration 2 are performed with Quantum espresso. The value of obtained Eg for SiCNT is agreement with obtained Eg with Gaussian at B3LYP/6-31G\*. as well as, the Fermi level (3.345 eV) is set between the top of the highest energy valence band and the bottom of the lowest energy conduction band. Therefore, SiCNT is a semiconductor. Our results indicate that the Eg slightly

decreases for configuration2, thus the electric conductivity of the SiCNT will not considerably change in the presence of CS<sub>2</sub>.

The DOS plots for studied configuration 2 and SiCNT are shown in Fig. 9. It is revealed from DOS plots that the valence and conduction levels shift upon adsorption process. Therefore, the electronic properties of the SiCNT are sensitive to the CS<sub>2</sub> molecule adsorption.

In recent years, the field emission properties of nanotubes have acquired great importance. The field emission property is significantly determined by the work function. The CS<sub>2</sub> adsorption changes the work function of the SiCNT and modifies its field emission properties. The emitted electron current densities are defined by the following equation:

$$J=AT^2\exp(-\Phi/KT) \quad (11)$$

Where A is the Richerdson constant (A/m<sup>2</sup>), T is the temperature (K) and  $\Phi$  is the material's work function.

It can be seen from Table 4, the work function is increased after absorbing the CS<sub>2</sub> molecule. This can be attributed to the shift LUMO and lowering of the Fermi level. Therefore, there is a positive change in the work function that indicates charge transfer between CS<sub>2</sub> and SiCNT.

According to equation 9, the emitted electron current density relates with the negative value of work function. Thus, there is decrease in the emitted electron current density from the SiCNT upon the adsorption process, which confirms its sensitivity towards CS<sub>2</sub> molecule. Our results indicate that for configurations 4 and 7, HOMO-LUMO gap differs between the B3LYP and B3LYP-D (see Table S3). From the results, the dispersion interaction cannot be ignored to consider molecular properties of these complexes by DFT calculations.

In order to investigate the changes of electronic structures in the SiCNT caused by adsorption of CS<sub>2</sub> molecule, the total density of states of the pristine SiCNT and CS<sub>2</sub>-SiCNT complexes are shown in Figure 9. For the pristine SiCNT, our CAM-B3LYP calculation obtains a band gap of 1.94 eV. In the configure2, when CS<sub>2</sub> molecule is chemically adsorbed on the nanotube surface, the value of band gap of the system increases by 0.19 eV. As well as, the work function is decreased after absorbing the CS<sub>2</sub> molecule.

### 3.6. NMR analysis

To study the effect of CS<sub>2</sub> adsorption on electronic structure properties of nanotube, the chemical shielding (CS) tensors at the sites of various C and Si atoms for different configurations are calculated and collected in Table 3.

To investigate the influence of tube –CS<sub>2</sub> molecule interaction on the <sup>13</sup>C and <sup>29</sup>Si NMR tensors, we assessed the C and Si chemical shielding isotropy values of nanotube before and after CS<sub>2</sub> adsorption.

In the pristine SiCNT, the C atoms that are terminated by H atoms have the largest value of the  $\sigma_{\text{iso}}$  (<sup>13</sup>C) parameter. The <sup>13</sup>C NMR isotropy value decreases along the tube axis, from C1-layer to C4-layer. For the Si nuclei, the largest value of the  $\sigma_{\text{iso}}$  belongs to the Si3-layer.

Our theoretical results indicate that CS<sub>2</sub> adsorption on the nanotube surface has a considerable influence on Si and <sup>13</sup>C NMR tensors. According to GIAO calculations performed after adsorption CS<sub>2</sub> molecule on nanotube, for figure 2 the isotropy value of Si NMR shielding tensor reduces, at the Si6 site. This can be explained by less electronic density at the site of this nucleus. In addition, the isotropy value of <sup>29</sup>Si and <sup>13</sup>C NMR shielding tensor increases, at the C1 and Si2. It is worth mentioning that just the electrostatic properties of these nuclei are mainly dependent on electronic density around the atoms. Therefore, by CS<sub>2</sub> adsorption, the electronic densities of nuclei Si and C and the CS parameters undergo changes.

### ***3.7. Molecular electrostatic potential***

The molecular electrostatic potential MEPs have been established as a guide to the prediction of molecular behavior. It is a useful tool in studying both electrophilic and nucleophilic processes.

For the pristine SiCNT, the end carbon atoms become negative by the electron-donating hydrogens. This can provide a better understanding of why the zigzag SiCNT reactivity is higher at the carbon end. The inside of the tube weakly is positive. The surfaces over the end silicon atoms are positive. It can be seen from fig. 10 that the CS<sub>2</sub> fragment is more positive in adsorbed form as compared to the free molecule, indicating a charge transfer from CS<sub>2</sub> molecule to SiCNT.

### ***3.8. Field effect on the structural parameters***

Due to variety of applications of electric field (EF) effects on the molecule, it is necessary to understand that how the molecule would respond to the electric field, thus, in the present study an investigation is made to explore the effect of the electric field on the adsorption process.

To investigate the external electric field effect on the structural properties of the SiCNT, we systematically analyze the changes of the bond length of tube under the external electric field. The structural parameters consist of the bond lengths for SiCNT and the configuration 2 when electrical field is applied in the perpendicular and parallel direction of the nanotube axis. Inspection of the theoretical results indicates that when EF is applied in the parallel direction of the tube axis, the bond lengths along the direction of the external field decrease gradually from  $1.839 \text{ \AA}$  at the field strength of the 0 to  $1.803 \text{ \AA}$  at the field strength of 0.005 a.u, while the other bonds increase. On the other hand, application external electric field in the perpendicular direction of the nanotube axis is caused that some of Si-C bonds stretched and the rest compressed.

The structure of the configuration 2 under the different external electric field is depicted in Fig 11. As it is evident from this figure, after applying an external electric field, the orientation of the adsorbed  $\text{CS}_2$  on the nanotube changed due to the polarization interaction. Obtained values of the adsorption energy decrease with an upward trend in the applied external electric field strengths. It can be concluded that adsorption of the  $\text{CS}_2$  molecule can be significantly weakened by using external electric field.

Computed total energy values of configuration 2 and pristine nanotube before and after applying an external EF indicate that the electronic energy reduces as electric field strength increases in both parallel and perpendicular directions, but the parallel electrical field leads to more stable complex.

Length of the nanotube can be considered as an important parameter characterizing its structural response to the applied parallel and perpendicular electric field in the nano-electronic circuit. Inspection of the theoretical results indicates that length of the nanotube changes slightly with an increase in the electric field strengths. Therefore, the length resistance of the nanotube against of the external electric field can be considered as an advantage of the nanotube in molecular scale device.

More insight into nanotube- $\text{CS}_2$  interaction can be obtained by examining the electron density. The charge density distribution map on the configuration2 in the presence of the different field is

shown in Fig 12. Weak coupling between CS<sub>2</sub> and the nanotube is found in the presence of the different fields.

### ***3.9. Electric field effect on the spatial distribution of the molecular orbitals***

Due to understand the electric response in the SiCNT, we investigate the electronic energies of the nanotube in the presence of the different applied parallel and perpendicular electric field strengths. The energy levels of the HOMO and LUMO of the pristine nanotube and configuration 2 under different electric field are collected in Table 5. As shown in this Table, under the external electric field the HOMO energy level moves down and the LUMO energy level insignificantly changes. Therefore the band gap increases with increasing strength of the electric field in both parallel and perpendicular directions to the nanotube axis. Inspection of the theoretical results indicates that under the interaction by the electric field in both parallel and perpendicular direction to the nanotube axis, the energy gap of the nanotube increased in comparison with the case no electric field. Therefore the adsorption energy of the CS<sub>2</sub> on the nanotube decreased. As is evident from Table 5, the applied parallel electric field has more influence on the molecular orbital of the nanotube than the applied perpendicular electric field.

### ***3.10. Diameter effect of the nanotube on the structural parameters and spatial distribution of the molecular orbitals***

In the present work, adsorption behaviors of the CS<sub>2</sub> on the single-walled SiCNT are studied by using the representative models of (6,0), (7,0) zigzag single walled SiCNT for the most stable configuration (configuration 2, Fig.13). It is obvious from Table S5, two types of bonds in each C-Si ring are least affected due to effect of diameter of the nanotube, therefore, change in diameter affects the C–Si bond strength.

Our results indicate that the stability of the complexes decreases as nanotube diameter increases. Therefore, the adsorption energy for (7,0) nanotube-CS<sub>2</sub> is lower than (6,0) nanotube-CS<sub>2</sub>. The nanotube-CS<sub>2</sub> distance shows considerable sensitivity to the type of the nanotube. This reveals from Table S5, the  $R_{\text{nanotube-CS}_2}$  is increased when moving from a small diameter (6,0) SiCNT to a larger (7,0) nanotube.

It is interest to study the variations in HOMO-LUMO energy gap in order to investigate the the CS<sub>2</sub>-sensing properties of SiCNT. Comparison of the DOS curves of the pristine (7,0) and

(6,0) SiCNT and CS<sub>2</sub>/SiCNT complex depicted in Fig. 15 shows that as nanotube diameter increases, E<sub>g</sub> enhances. Therefore, different CS<sub>2</sub> –sensing behavior can be expected for small and large size SiCNT. LUMO and HOMO profiles of the (7,0) and (6,0) SiCNT is shown in Fig. 14. Isosurface plots for HOMO and LUMO levels of (7,0) and (6,0) SiCNT show that as nanotube diameter increases, LUMO contributions at nanotube end decrease. Therefore, it is expected that the CS<sub>2</sub> molecule interaction with nanotube decrease, as the diameter of nanotube increase.

#### 4. Conclusion

The calculations for pristine nanotube have been performed using two different computational code that results of these two different computational code are agreement with together. As well as, in this work we present a theoretical study on the adsorption of CS<sub>2</sub> molecules onto the interior and exterior surfaces of SiCNT. We consider two symmetric categories of adsorption configuration; one in which CS<sub>2</sub> molecule places parallel to SiCNT surface and the other in which CS<sub>2</sub> molecule places perpendicular to SiCNT surface. Based on the results, we can say that the adsorption of CS<sub>2</sub> molecule onto exterior SiCNT is energetically favorable and formed complexes are quite stable, while the situation is vice versa for internal surface of the nanotube. Our theoretical results indicate that the adsorption energy values vary from -163.99 to 885.39 KJ/mol. These values confirm that the CS<sub>2</sub> molecule can be adsorbed physically or chemically on the external surface of the nanotube as well as it can be chemically adsorbed on the internal surface of the nanotube. Geometrical structures, electronic properties, the Wiberg bond index and the donor–acceptor interactions in the NBO basis are analyzed to predict the adsorption behavior of CS<sub>2</sub> molecule. The results of the NBO analysis illustrate that in the studied complexes, the nanotube acts as an electron acceptor and CS<sub>2</sub> molecule behaves as electron donor. It can be seen from DOS plots that the electronic properties of the SiCNT are sensitive to the CS<sub>2</sub> molecule adsorption.

#### Acknowledgements

The authors would like to thank Dr. Sarhaddi (University of Birjand) for valuable and useful discussions during the course of this work as well as we perform some calculations with Saffron HPC cluster .

## Reference

- [1] R.O. Beauchamp Jr, J.S. Bus, J.A. Popp, C.J. Boreiko, L. Goldberg, M.J. Mckenna, *Critic. Rev. Toxicol*, 1983, **11**, 169.
- [2] R. Wang, D. Zhang, *Aust. J. Chem*, 2008, **61**, 941.
- [3] A. Ahmadi Peyghan, A. Omidvar, N.L. Hadipour, Z. Bagheri, M. Kamfiroozi, *Physica E*, 2012, **44**, 1357.
- [4] J. Kong, N.R. Franklin, C. Zhou, M.G. Chapline, S. Peng, K. Cho., H. Dai, *Scie*, 2000, **287** 622.
- [5] P.G. Collins, K. Bradley, M. Ishigami, A. Zettl, *Science*, 2000, **287**, 1801.
- [6] H. Raissi, F. Mollania, *Eur. J. Pharm. Sci*, 2014, **56**, 37.
- [7] M. Chi, Y.P. Zhao, *Comp. Mater. Sci*, 2009, **46**, 1085.
- [8] Zhu X, ZhaoYP, *J.Phys.Chem.C*, 2014, **118**, 17737.
- [9] J. Y. Fan, X. L. Wu, K. C. Paul, *Prog Mater Sci* , 2006, **51**, 983.
- [10] P. Melinon, B. Masenelli, F. Tournus, A. Perez, *Nat Mater*, 2007, **6**, 479.
- [11] B. K. Teo, X. H. Sun, *Chem. Rev*, 2007, **107**, 1454.
- [12] B. K. Teo, S. P. Huang, R. Q. Zhang, W. K. Li, *Coord. Chem. Rev*, 2009, **253**, 2935.
- [13] M. Menon, E. Richter, A. N. Andriotis, *Phys. Rev B*, 2004, **69**, 115322.
- [14] M. Zhao, Y. Xia, F. Li, RQ. Zhang, ST. Lee, *Phys. Rev. B*, 2005, **71**, 085312/1.
- [15] A. D. Patrick, X. Dong, T. C. Allison, E. B. Barojas, *J. Chem. Phys*, 2009, **130**, 244704/1.
- [16] Z. Wang, F. Gao, J. Li, X. Zu, WJ. Weber, *Nanotechnology*, 2009, **20**, 075708/1.
- [17] J. M. Zhang, L. Y. Chen, S. F. Wang, K. W. Xu, *Eur Phys J B*, 2010, **73**, 555.
- [18] Y. u. Ming, C.S. Jayanthi, and S.Y. Wu, *Phys. Rev. B*, 2010, **82**, 075407/1.
- [19] K. M. Alam, A. K. Ray, *Phys. Rev. B*, 2008, **77**, 035436/1.
- [20] J. X. Zhao, Y. H. Ding, *J Chem Theory Comput*, 2009, **5**, 1099.
- [21] R. Q. Wu, M. Yang, Y. H. Lu, Y. P. Feng, Z. G. Huang, Q. Y. Wu, *J. Phys. Chem. C*, 2008, **112**, 15985.
- [22] G. Mpourmpakis, G. E. Froudakis, G. P. Lithoxoos, j.Samios, *J Nano Lett*, 2006, **6**, 1581.
- [23] J. X. Zhao, B. Xiao, Y. H. Ding, *J. Phys. Chem. C*, 2009, **113**, 16736.
- [24] L. Wang, J. Lu, G. F. Luo, W. Song, L. Lai, M.W. Jing, R. Qin, J. Zhou, Z. X. Gao, W. N. Mei, *J. Phys. Chem. C*, 2007, **111**, 18864.

- [25] I. J. Wu, G.Y. Guo, *Phys. Rev. B*, 2007, **76**, 035343.
- [26] P. Hohenberg, W. Kohn, *Phys. Rev.*, 1964, **136**, 864.
- [27] A. D. Beck, *J. Chem. Phys.*, 1993, **98**, 5648.
- [28] T. Yanaia, D. P. Tew, N. C. Handy, *Chem. Phys. Lett.*, 2004, **393**, 51.
- [29] S. Grimme, *J. Comput. Chem.*, 2004, **12**, 1463.
- [30] S. B. Boys, F. Bernardi, *Mol. Phys.*, 1970, **19**, 553.
- [31] T. A. Koopmans, *Physica*, 1934, **1**, 104.
- [32] R. G. Pearson, *J. Am. Chem. Soc.*, 1985, **107**, 6801.
- [33] R. G. Parr, P. K. Chattaraj, *J. Am. Chem. Soc.*, 1991, **113**, 1854.
- [34] A. E. Reed, L. A. Curtiss, F. Weinhold, *Chem. Rev.*, 1988, **88**, 899.
- [35] E. D. Glendening, A. E. Reed, J. E. Carpenter, F. Weinhold, NBO Version 3.1, Gaussian, Inc., Pittsburgh PA, 1992.
- [36] M. J. Frisch, G. W. Trucks, H. B. Schlegel, G. E. Scuseria, M. A. Robb, J. R. Cheeseman, J. A. Montgomery, T. Vreven, K. N. Kudin, J. C. Burant, J. M. Millam, S. S. Iyengar, J. Tomasi, V. Barone, B. Mennucci, M. Cossi, G. Scalmani, N. Rega, G. A. Petersson, H. Nakatsuji, M. Hada, M. Ehara, K. Toyota, R. Fukuda, J. Hasegawa, M. Ishida, T. Nakajima, Y. Honda, O. Kitao, H. Nakai, M. Klene, X. Li, J. E. Knox, H. P. Hratchian, J. B. Cross, V. Bakken, C. Adamo, J. Jaramillo, R. Gomperts, R. E. Stratmann, O. Yazyev, A. J. Austin, R. Cammi, C. Pomelli, J. W. Ochterski, P. Y. Ayala, K. Morokuma, G. A. Voth, P. Salvador, J. J. Dannenberg, V. G. Zakrzewski, S. Dapprich, A. D. Daniels, M. C. Strain, O. Farkas, D. K. Malick, A. D. Rabuck, K. Raghavachari, J. B. Foresman, J. V. Ortiz, Q. Cui, A. G. Baboul, S. Clifford, J. Cioslowski, B. B. Stefanov, G. Liu, A. Liashenko, P. Piskorz, I. Komaromi, R. L. Martin, D. J. Fox, T. Keith, M. A. Al-Laham, C. Y. Peng, A. Nanayakkara, M. Challacombe, P. M. W. Gill, B. Johnson, W. Chen, M. W. Wong, C. Gonzalez, J. A. Pople, Gaussian 03, Revision C. 02, Gaussian, Inc.: Wallingford, CT, 2004.
- [37] M. Wendt, F. Weinhold, NBOView 1.0; Theoretical Chemistry Institute, University of Wisconsin: Madison, WI. 2001.
- [38] R. F. W. Bader, A. Streitwieser, A. Neuhaus, K. F. Laidig, P. Speers, *J. Am. Chem. Soc.* 1996, **118**, 4959.
- [40] F. Biegler-König, J. Schönbohm, *J. Comput. Chem.* 2002, **23**, 1489.

- [38] M. K. Cyran' ski, T.M. Krygowski, A. R. Katritzky, P. v. R. Schleyer, *J. Org. Chem*, 2002, **67**, 1333.
- [41] A.W. Ehlers, E.J. Baerends, K. Lammertsma, *J. Am. Chem. Soc*, 2002, **124**, 2831.
- [42] K.K. Pandey, G. Frenking, *Eur. J. Inorg. Chem.* 2004, **2004**, 4388.
- [43] P. Giannozzi, S. Baroni, N. Bonini, M. Calandra, R. Car, C. Cavazzoni, D. Ceresoli, G. L. Chiarotti, M. Cococcioni, I. Dabo, A. D. Corso, S. de Gironcoli, S. Fabris, G. Fratesi, R. Gebauer, U. Gerstmann, C. Gougoussis, A. Kokalj, M. Lazzeri, L. Martin-Samos, N. Marzari, F. Mauri, R. Mazzar-ello, S. Paolini, A. Pasquarello, L. Paulatto, C. Sbraccia, S. Scandolo, G. Sclauzero, A. P. Seitsonen, A. Smogunov, P. Umari, and R. M. Wentzco-vitch, *J. Physics: Condens. Matter*, 2009, **21**, 395502.
- [44] J. P. Perdew, Y. Wang, *Phys. Rev B*, 1992, **45**, 13244.
- [45] Q. Yuan, Y. P. Zhao, L. Li, T. Wang, *J. Phys. Chem. C*, 2009, **113**, 6107.

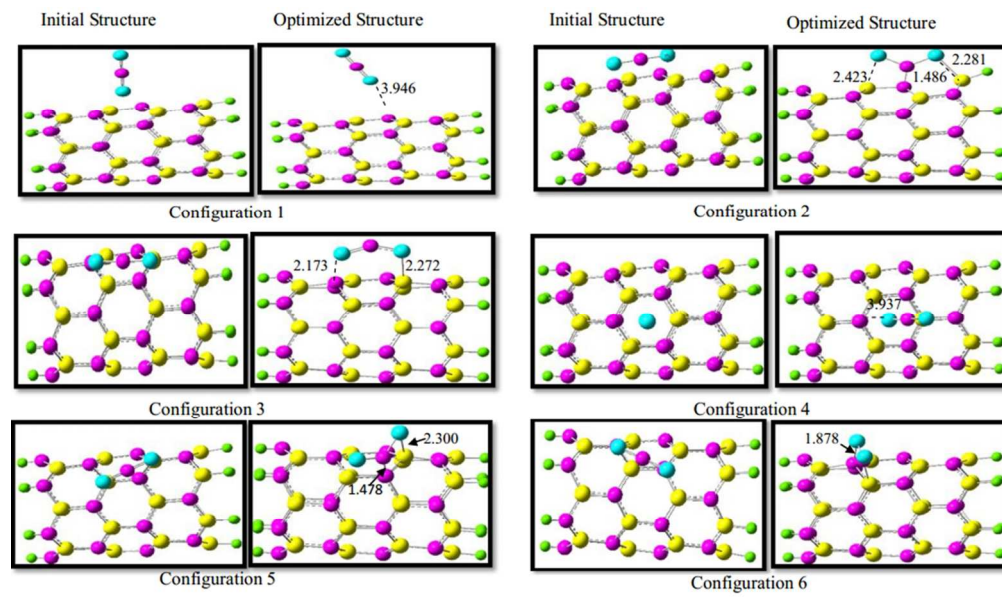
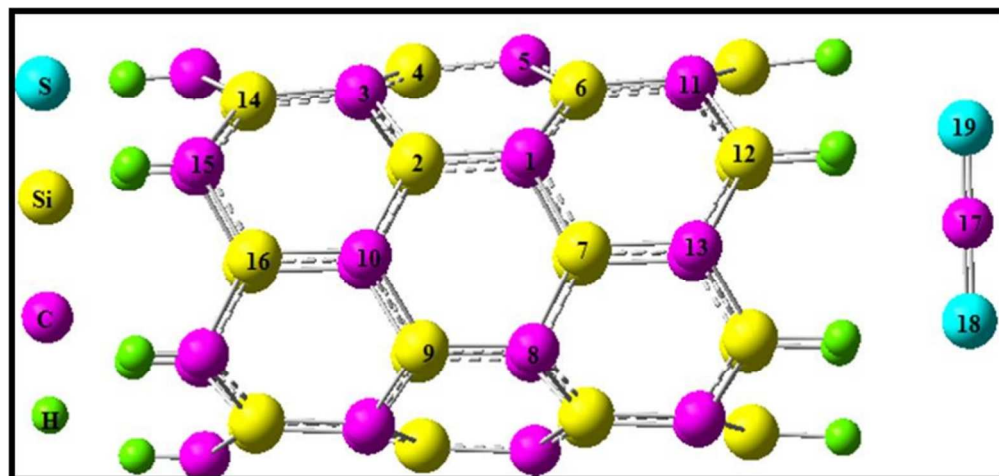


Fig. 2 Initial and optimized structures for different configurations

160x98mm (300 x 300 DPI)



**Fig. 1** Optimized geometry for zigzag (6,0) silicon-carbide nanotube

143x78mm (300 x 300 DPI)

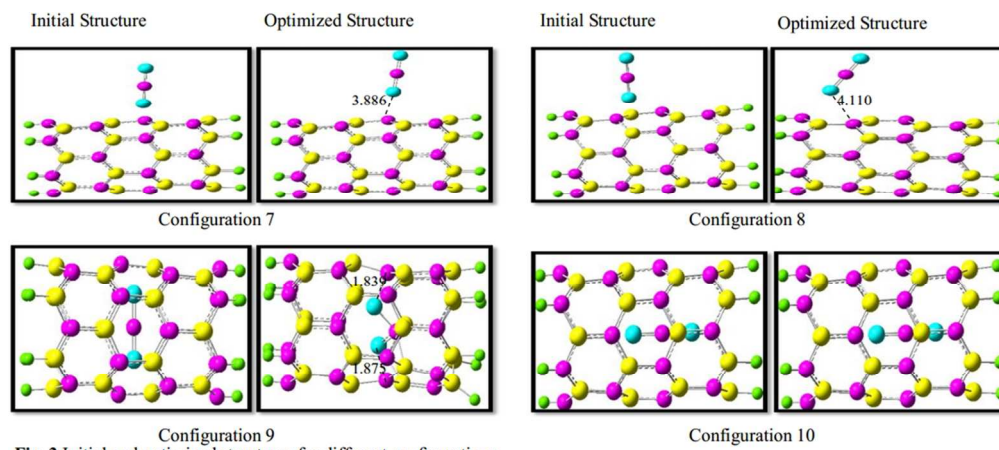


Fig. 3 Initial and optimized structures for different configurations

135x61mm (300 x 300 DPI)



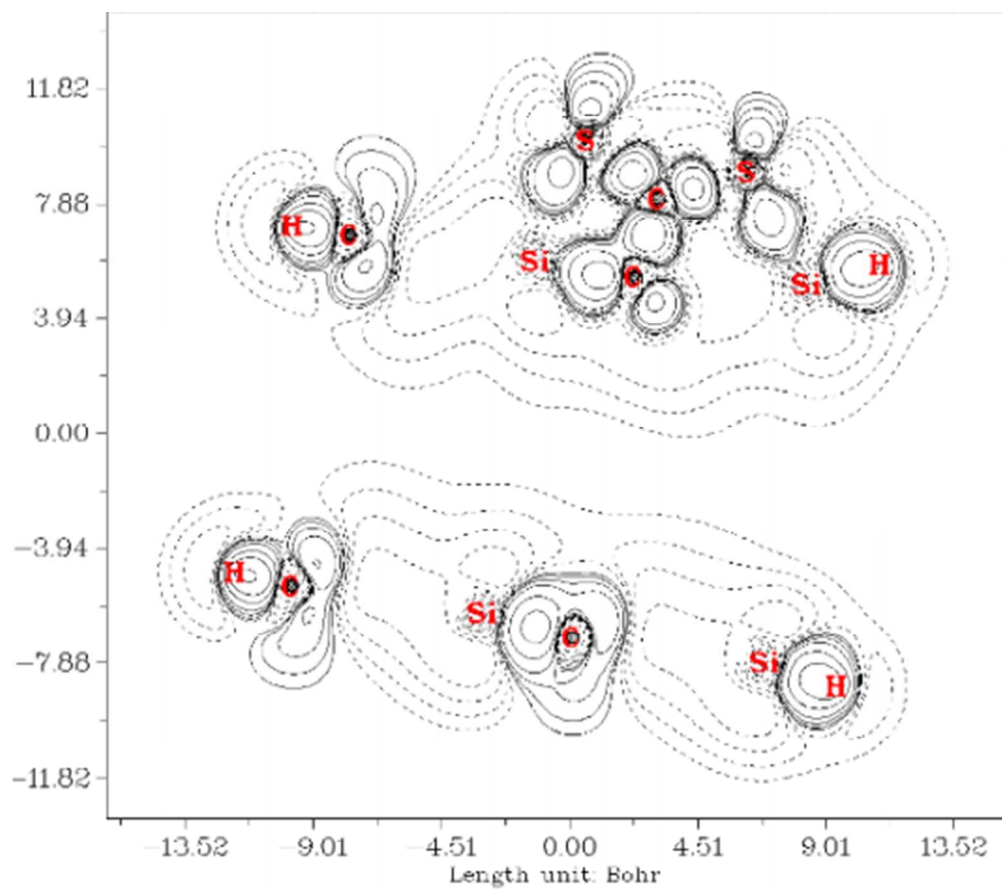


Fig5. Deformation density map for the configuration 2.

160x182mm (300 x 300 DPI)

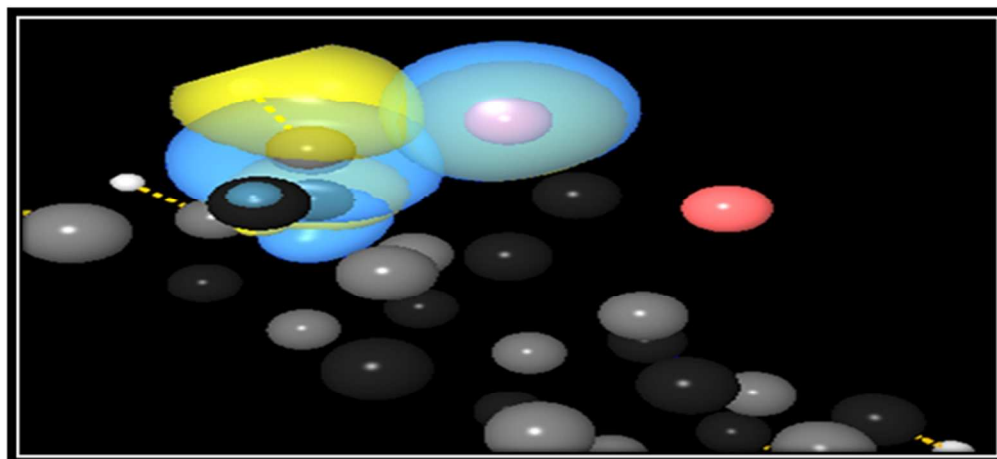
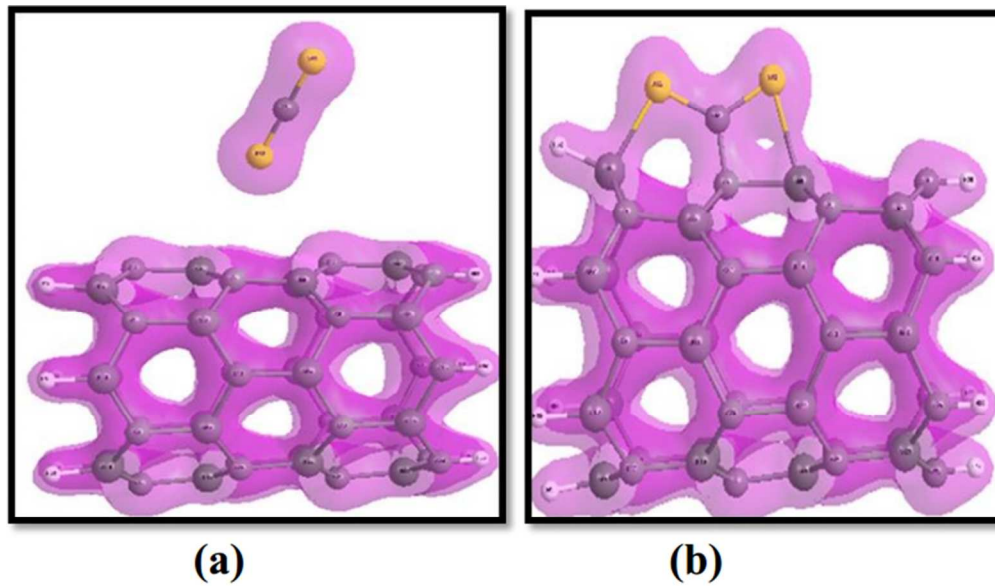


Fig. 6 NBO contour plot illustrating the interaction between lone pair Orbitals of S atom of  $\text{CS}_2$  with  $\sigma^*$ Si12-C13 of the nanotube in configuration 2

117x68mm (300 x 300 DPI)



**Fig. 7** Isosurface of the total electron density for (a) configuration 2  
(b) configuration 1 where 0.05 was used as an isovalue of total electron density

149x107mm (300 x 300 DPI)

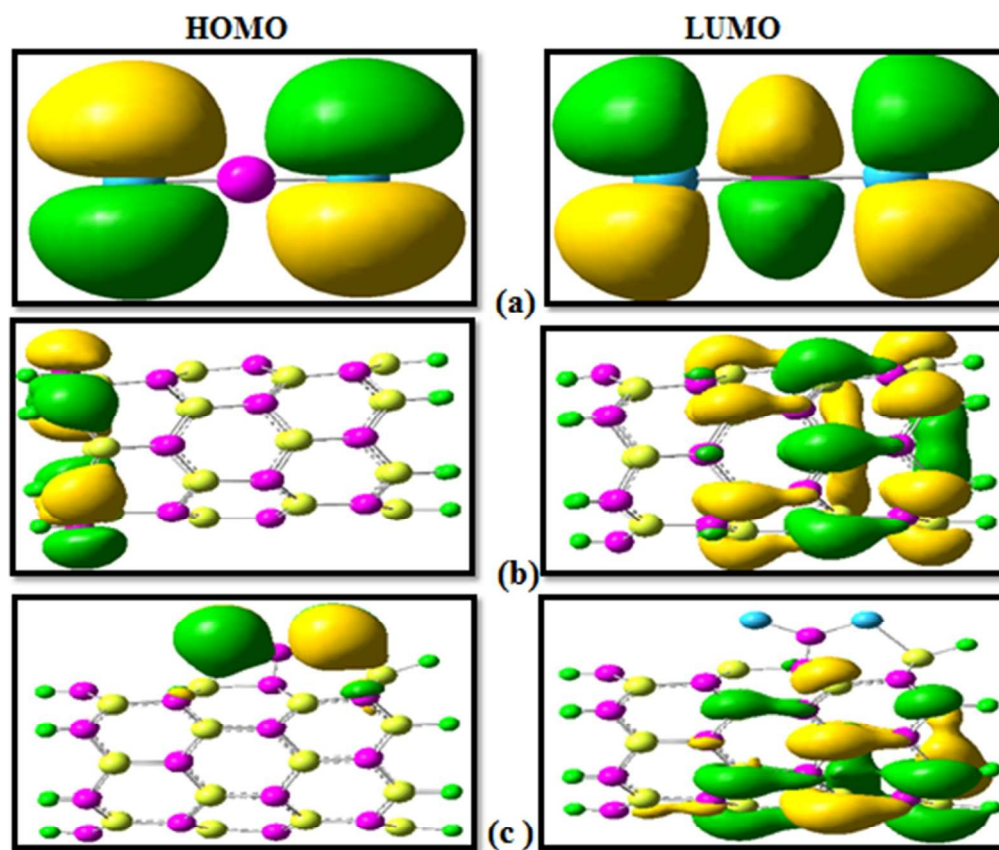


Fig. 8 Orbital depiction of HOMO and LUMO in (a) CS<sub>2</sub> molecule (b) SiCNT (c) Configuration 2 optimized at B3LYP/6-31G\*

124x114mm (300 x 300 DPI)

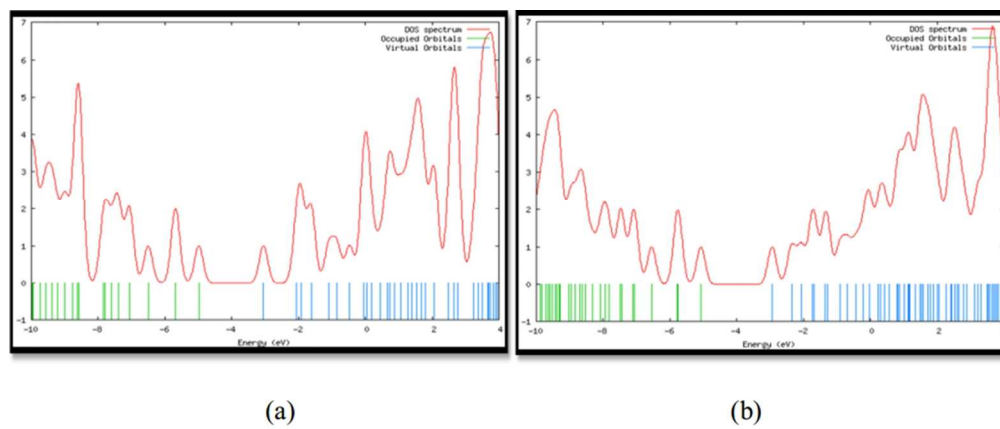
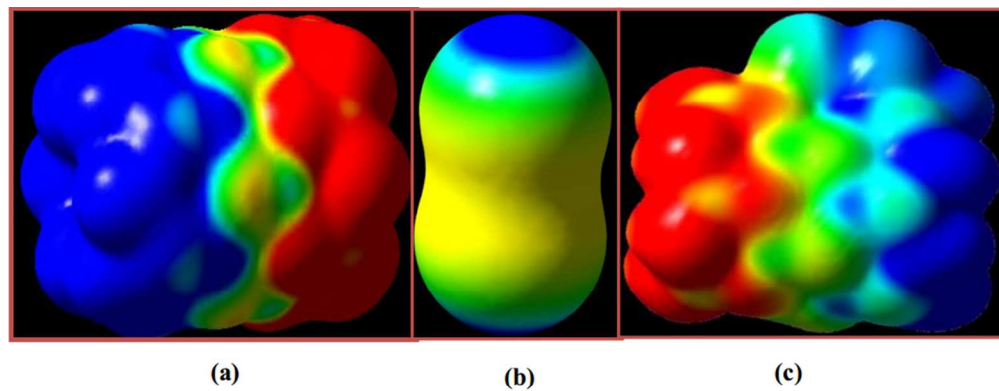


Fig. 9 Calculated density of states for (a) SiCNT (b) Configuration 2 at CAM-B3LYP.

130x61mm (300 x 300 DPI)



**Fig. 10** Molecular electrostatic plots for (a) SiCNT, (b) CS<sub>2</sub> molecule and (c) Configuration 2

132x62mm (300 x 300 DPI)

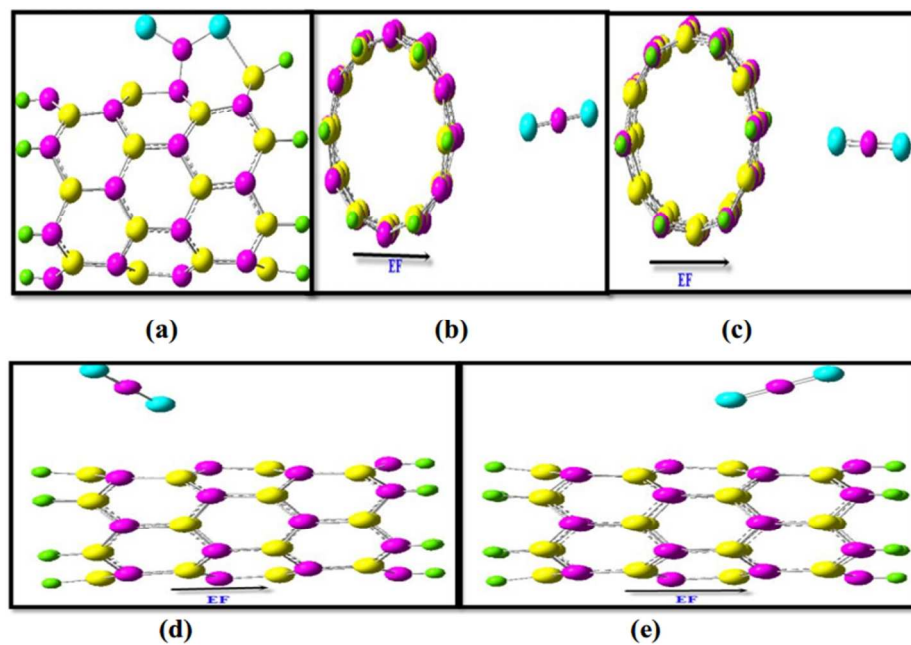


**Fig. 11** The full optimized structure of (a) SiCNT/CS<sub>2</sub> complex (configuration 2), (b and c) Configuration2 under the electric field of 0.0025 and 0.0050 a.u. in perpendicular and (d) and (e) under the electric field of 0.0025 and 0.0050 a.u. in parallel direction to the SiCNT axis, respectively. The arrow indicates the direction of the applied external electric field.

167x121mm (300 x 300 DPI)

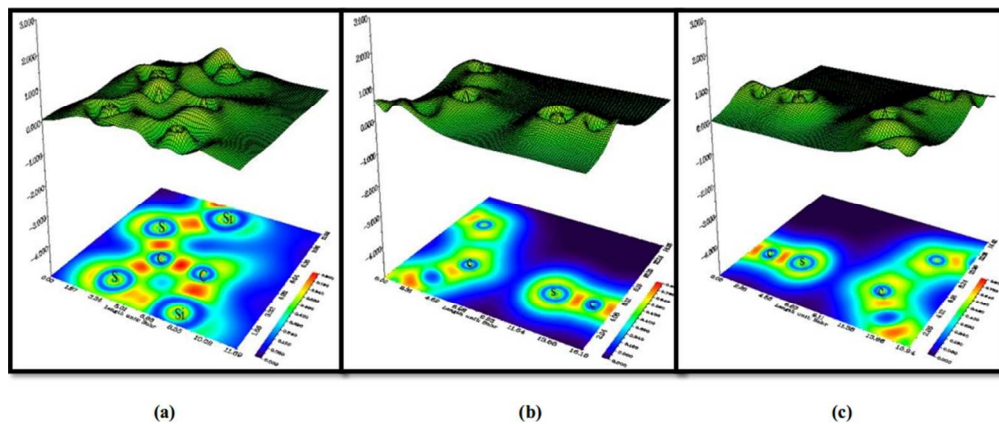


**Fig. 12** The contour plot of electron density for (a) Configuration 2 and (b and c) Configuration2 under the electric field of 0.0025 and 0.0050 a.u. in perpendicular direction to the SiCNT axis, respectively

137x67mm (300 x 300 DPI)

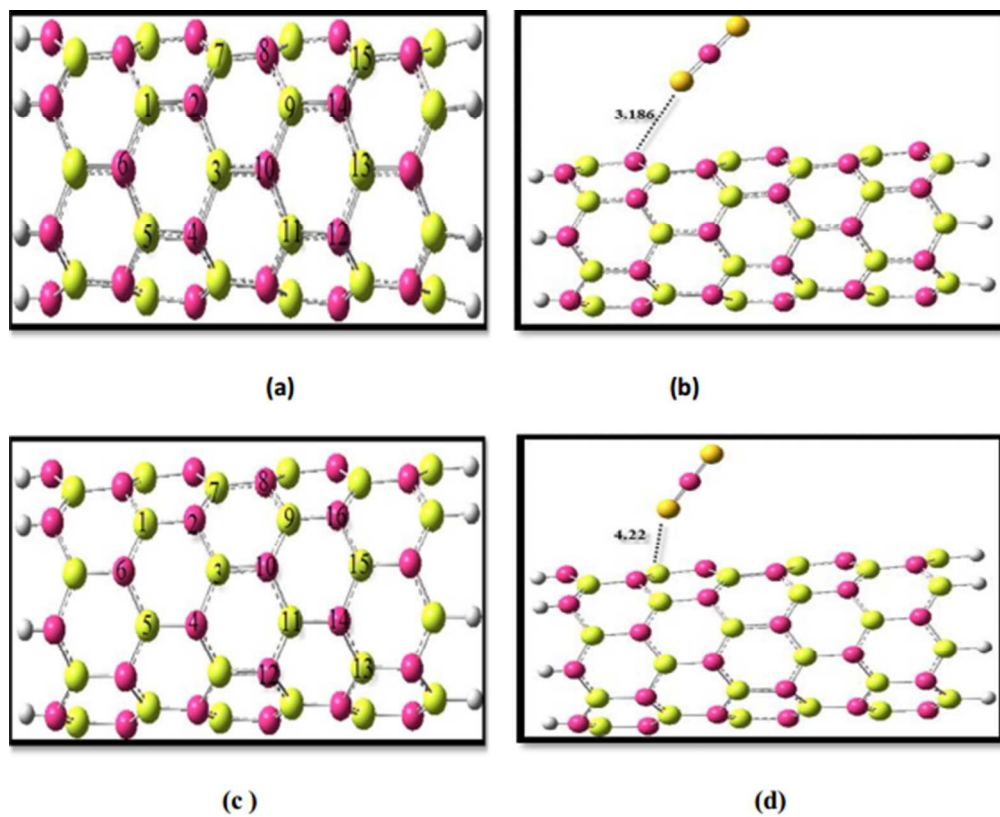


**Fig. 13** Optimized geometry for (a) (6,0) SiCNT (b) CS<sub>2</sub>-(6,0) SiCNT (c) (7,0) SiCNT (d) CS<sub>2</sub>-(7,0) SiCNT at CAM-B3LYP

154x147mm (300 x 300 DPI)

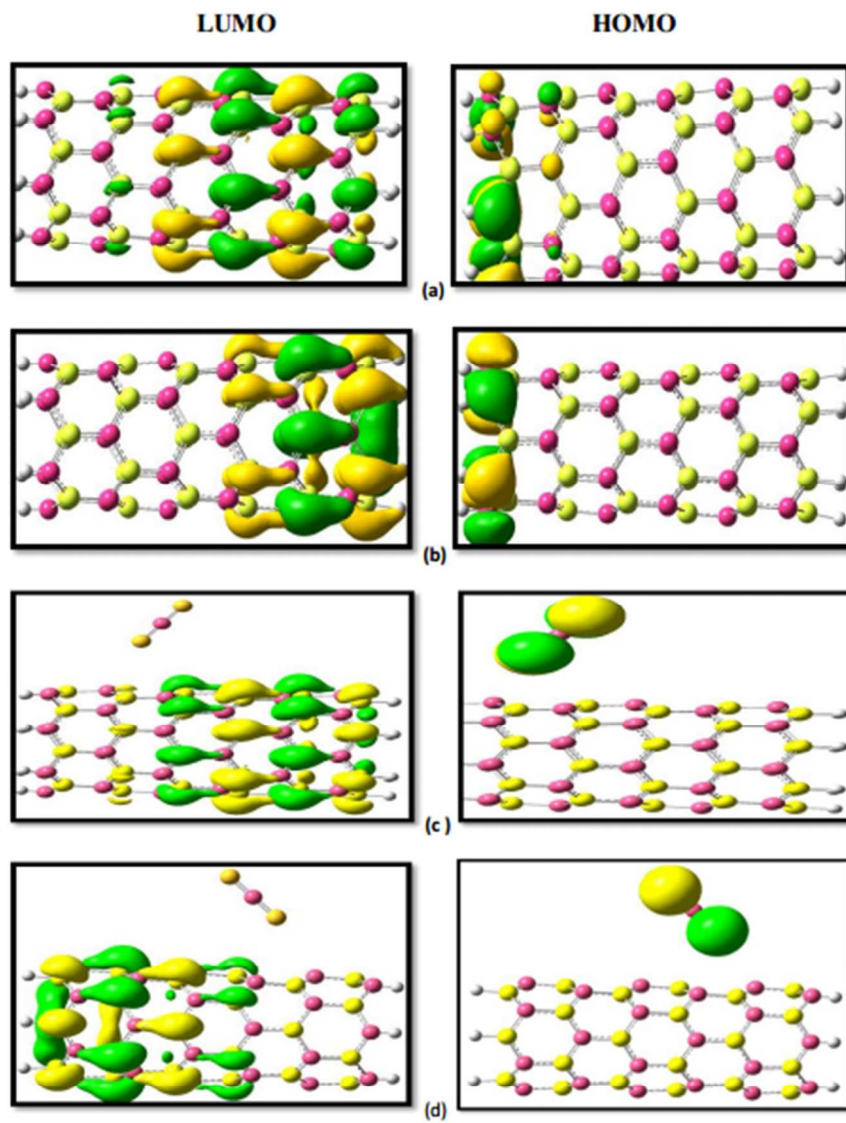


**Fig. 14** Orbital depiction of HOMO and LUMO in (a) (7,0) SiCNT (b) (6,0) SiCNT (c) CS<sub>2</sub>-(7,0) SiCNT (d) CS<sub>2</sub>-(6,0) SiCNT optimized at CAM-B3LYP/6-31G\*

167x232mm (300 x 300 DPI)

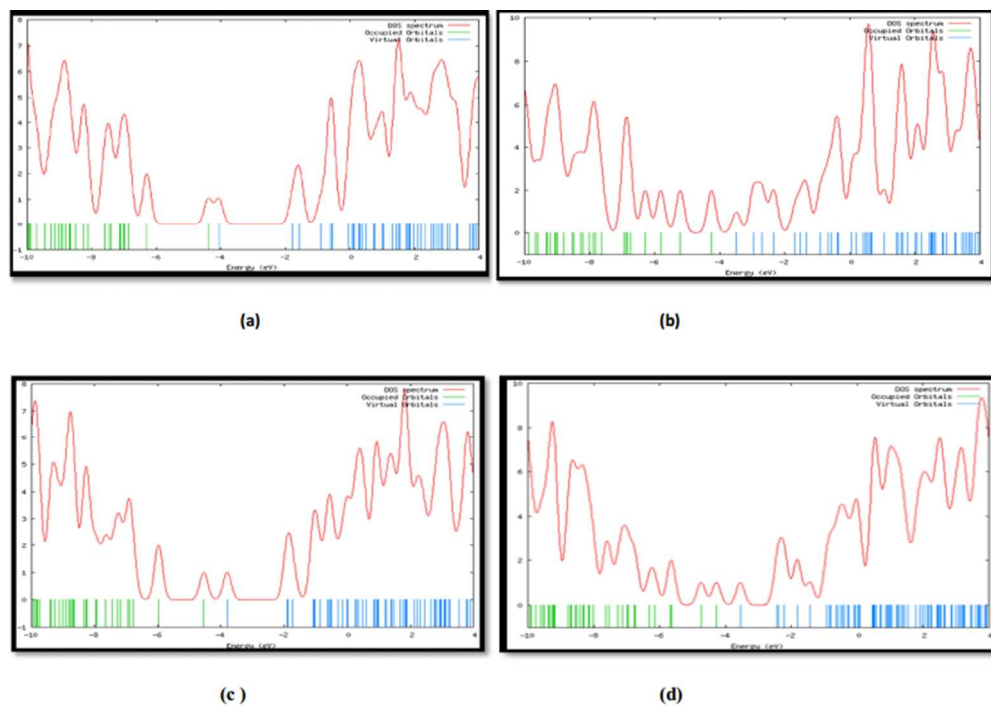


**Fig. 15** Calculated density of states for (a) (6,0)SiCNT (b) (7,0)SiCNT (c) CS<sub>2</sub>-(6,0)SiCNT (d) CS<sub>2</sub>-(7,0)SiCNT at CAM-B3LYP.

157x117mm (300 x 300 DPI)

**Table 1** The geometrical parameters (bond lengths (R) is in Å), adsorption ( $E_{ad}$ ), interaction ( $E_{int}$ ) and deformation ( $E_{def}$ ) energies ( $\text{kJmol}^{-1}$ ) and stretching frequencies ( $\nu$ , in  $\text{cm}^{-1}$ ) of nanotube...CS<sub>2</sub> contact calculated at the B3LYP/6-31G\* level

	$R_{C-Si}$	$R_{CS_2 \dots nanotube}$	$R_{C-S}$	$\theta_{S-C-S}$	$\nu_{C=S}$	$E_{ad}$	$E_{int}$	$E_{def}$
Configuration 1	C4-Si5=1.815 C5-Si6=1.789	C5...S18=3.946	C17-S19=1.564 C17-S18=1.564	179.89	1553.17	-40.29	-5.91	-34.38
Configuration 2	C5-Si4=1.945 C5-Si6=1.907	C5...C17=1.486 Si4...S18=2.423	C17-S19=1.738 C17-S18=1.694	125.24	1027.99	-163.98	-505.19	341.03
Configuration 3	C1-Si2=1.790 C1-Si6=1.851	Si6...S18=2.272	C17-S19=1.578 C17-S18=1.666	144.391	1231.55	15.41	-119.17	134.58
Configuration 4	C1-Si2=1.814 Si2-C10=1.791	S19...C10=3.937 S19...Si7=4.065	C17-S19=1.563 C17-S18=1.565	179.997	1549.47	-41.58	-7.199	-34.38
Configuration 5	C1-Si2=1.975 C1-Si6=1.952	C1...C17=1.478 Si6...S19=2.300	C17-S19=1.729 C17-S18=1.708	127.045	1043.80	-66.24	-350.61	284.38
Configuration 6	C1-Si2=1.857 C3-Si2=2.04	Si2...C17=1.931 C3...S18=1.878	C17-S19=1.625 C17-S18=1.792	127.598	1162.78	-29.49	-304.64	275.14
Configuration 7	C5-Si4=1.815 C5-Si6=1.789	C5...S19=3.886	C17-S19=1.564 C17-S18=1.564	179.902	1552.31	-40.77	-6.36	-34.41
Configuration 8	C1-Si2=1.815 Si2-C3=1.788	C3...S18=4.110	C17-S19=1.566 C17-S18=1.562	179.9794	1551.35	-39.63	-5.96	-33.67
Configuration 9	C5-Si4=1.904 Si6-C5=1.938	S19...C5=1.839	C17-S19=1.661 C17-S18=1.741	89.59	962.53	885.39	161.61	723.79
Configuration 10	C1-Si7=1.811	S18...Si7=3.130	C17-S19=1.542 C17-S18=1.579	179.424	1524.41	287.86	301.01	-13.16

**Table 2** Topological properties (in au) of different configurations calculated at the B3LYP/6-31G\* level.

	$\rho$	$\nabla^2\rho$	$\rho$	$\nabla^2\rho$	$\rho$	$\nabla^2\rho$	G	V	H
	C-S		C-Si				Tube...CS2		
Configuration 1	C17-S19=0.24112 C17-S18=0.24093	0.427 0.4302	C4-Si5=0.12265 C4-Si6=0.12704	0.35984 0.3846	C5...S18=0.00314	0.00924	0.00173	-0.00116	0.000575
Configuration 2	C17-S19=0.20453 C17-S18=0.21692	-0.40084 -0.3522	C5-Si4=0.10273 C5-Si6=0.10803	0.20316 0.21164	C5...C17=0.25943 Si4...S18=0.06069	-0.57368 -0.03244	0.20739 0.021503	-0.5582 -0.05111	-0.35081 -0.02961
Configuration 3	C17-S19=0.24564 C17-S18=0.22077	-0.08824 -0.35236	C1-Si2=0.12793 C1-Si6=0.11673	0.39699 0.29094	Si6...S18=0.08256 C3...S18=0.08730	-0.01979 0.02023	0.041649 0.0527	-0.08824 -0.10034	-0.0466 -0.04764
Configuration 4	C17-S19=0.24112 C17-S18=0.24069	0.43632 0.41828	C1-Si2=0.12289 C10-Si2=0.12662	0.36352 0.38352	C10...S19=0.00331 Si7...S19=0.00307	0.00921 0.00784	0.001747 0.001493	-0.00119 -0.00103	0.000557 0.000467
Configuration 5	C17-S19=0.20829 C17-S18=0.21182	-0.41332 -0.38796	C1-Si2=0.09549 C1-Si6=0.10247	0.14768	C1...C17=0.26487 Si6...S19=0.07641	-0.58787 -0.0202	0.215685 0.036139	-0.57834 -0.07732	-0.36265 -0.04119
Configuration 6	C17-S19=0.23036 C17-S18=0.18885	0.02524 -0.29262	C1-Si2=0.11399 C3-Si2=0.09204	0.29912 0.13832	Si2...C17=0.10697 C3...S18=0.15643	0.21496 -0.18264	0.105043 0.099954	-0.15634 -0.24557	-0.0513 -0.14562
Configuration 7	C17-S19=0.24077 C17-S18=0.24106	0.43074 0.42616	C5-Si4=0.12264 C5-Si6=0.12705	0.35992 0.38464	C5...S19=0.00339	0.00984	0.001858	-0.00126	0.000599
Configuration 8	C17-S19=0.24045 C17-S18=0.24149	0.41524 0.44024	C3-Si2=0.12728	0.39048	C3...S18=0.00295	0.00828	0.001552	-0.00104	0.000515
Configuration 9	C17-S19=0.23978 C17-S18=0.20285	-0.51145 -0.3513	C5-Si4=0.10911 Si6-C5=0.10155	0.23079 0.19799	C5...S19=0.17173	-0.20008	0.118999	-0.28802	-0.16902
Configuration 10	C17-S19=0.25195 C17-S18=0.23781	0.48784 0.33419	C1-Si7=0.12494	0.37308	Si7...S18=0.01696	0.03373	0.008837	-0.00924	-0.00041

**Table 3**  $E^{(2)}$  (Kcal/mol) corresponds to charge transfer and some NMR data (ppm) computed at the B3LYP/6-31G\* level of theory

Donor→acceptor	$E^{(2)}$	Bond order	Bond order	$\sigma_{iso}$	$\Delta\sigma$	
Configuration 1	LPS18→LP*Si4	0.6	C17-S18=1.9840	C5-Si4=0.8381	C5=120.7429	96.3877
			C17-S19=1.9828	Si6-C5=0.9529	Si4=311.8533	113.1112
				C1-Si6=0.9584		
Configuration 2	LPS18→ $\sigma^*$ C5-C17	2.54	C17-S18=1.4709	C5-Si4=0.5489	C5=112.5661	31.6991
	LPS19→ $\sigma^*$ C5-C17	4.48	C17-S19=1.2691	C5-Si6=0.6207	Si4=393.2848	157.3414
Configuration 3	LPC17→ $\sigma^*$ C3-S19	66.45	C17-S18=1.4358	C1-Si2=0.9335	Si6=409.6517	13.0766
	LPC1→ $\sigma^*$ Si6-S18	9.31	C17-S19=1.9247	Si2-C3=0.7354	C1=133.2975	71.8182
	LPS18→ $\sigma^*$ Si6-C5	4.75		C1-Si6=0.7319	Si2=275.0149	145.3918
Configuration 4	LPS19→ $\pi^*$ Si7-C8	0.41	C17-S18=1.9709	C1-Si2=0.8408	C1=119.8620	96.0105
			C17-S19=1.9920	Si2-C10=0.9677	Si2= 311.9286	113.9848
					C10= 123.7548	97.5159
Configuration 5	$\pi$ C17-S18→ $\pi^*$ C3-Si2	56.91	C17-S18=1.3633	C1-Si2=0.5247	C1=104.9930	114.3899
	$\pi$ C17-S18→ $\sigma^*$ C3-Si2	7.91	C17-S19=1.2966	C1-Si6=0.5540	Si2=395.3113	214.427
	$\sigma$ C17-S18→ $\pi^*$ C3-Si2	12.14			Si6=432.3900	175.1585
Configuration 6	LPS19→ $\sigma^*$ Si2-C17	8.1	C17-S18= 1.1131	C1-Si2= 0.7115	C3=138.8656	37.9609
	LPS18→ $\sigma^*$ Si2-C17	3.88	C17-S19= 1.8128	Si2-C3= 0.5240	Si2=415.9419	77.6374
					C1=120.6785	105.3775
Configuration 7	LPS19→ $\pi^*$ C1-Si6	0.06	C17-S18=1.9826	C5-Si4=0.8409	C5=120.9960	94.9315
			C17-S19=1.9843	C5-Si6=0.9520	Si4=311.3241	113.4385
				Si6-C1=0.9594		
Configuration 8	LPS18→LP*Si2	0.5	C17-S18= 1.3336	Si2-C3=0.9647	C3= 123.0534	98.4466
	$\pi$ C17-S18→LP*Si2	0.43	C17-S19= 1.3223	C3-Si14= 0.8294	Si14= 279.8101	132.1797
				C1-Si2= 0.8384	Si2= 311.1161	116.2266
Configuration 9	LPC17→LP*Si6	168.61	C17-S18=1.0062	C5-Si4=0.6541	C5=108.8420	59.6722
			C17-S19=1.2400	C5-Si6=0.6221	Si4=326.1542	99.8191
Configuration 10	LPS18→LP*C3-Si14	7.03	C17-S18=1.6462	C5-Si4=0.8614	C5=120.7953	86.6811
			C17-S19=1.8692		Si4=303.2425	130.1896

**Table 4** Changes in thermodynamic functions ( $\text{kJmol}^{-1}$ ) upon complex formation, energy of the highest occupied molecular orbital ( $E_{\text{HOMO}}$ ), energy of the lowest unoccupied molecular orbital ( $E_{\text{LUMO}}$ ), the molecular orbital energy gap,  $E_g$ , Chemical hardness ( $\eta$ ) and chemical potential ( $\mu$ ), Fermi level energy and work function ( $\Phi$ ) in terms of eV computed.

	$E_{\text{HOMO}}$	$E_{\text{LUMO}}$	$E_g$	$\eta$	$\mu$	$E_{\text{FL}}$	$\Phi$	$\Delta G$	$\Delta H$	$T\Delta S$
SiCNT	-4.15534	-3.79739	0.35795	0.17898	-3.97637	-3.97637	3.97637	.....	.....	.....
Configuration1	-4.24075	-3.87382	0.36693	0.183465	-4.05729	-4.05729	4.05729	-21.3575	-37.9572	-16.5997
Configuration 2	-4.15997	-3.84608	0.31389	0.156945	-4.00303	-4.00303	4.00303	-137.907	-186.456	-48.5494
Configuration 3	-4.23069	-3.87355	0.35714	0.17857	-4.05212	-4.05212	4.05212	48.55206	3.720264	-44.8318
Configuration 4	-4.24048	-3.87382	0.36666	0.18333	-4.05715	-4.05715	4.05715	-21.1138	-38.282	-17.1682
Configuration 5	-4.22661	-3.87246	0.35415	0.177075	-4.04954	-4.04954	4.04954	-39.2383	-85.3617	-46.1234
Configuration 6	-4.32698	-3.97147	0.35551	0.177755	-4.14923	-4.14923	4.14923	-0.05764	-44.6589	-44.6012
Configuration 7	-4.24157	-3.87518	0.36639	0.183195	-4.05838	-4.05838	4.05838	-21.1138	-38.282	-17.1682
Configuration 8	-4.24864	-3.88334	0.3653	0.18265	-4.06599	-4.06599	4.06599	-7.91735	-41.963	-34.0457
Configuration 9	-4.34466	-3.97066	0.374	0.187	-4.15766	-4.15766	4.15766	310.0683	-258.4954	-51.5728
Configuration 10	-4.56878	-4.15534	0.41344	0.20672	-4.36206	-4.36206	4.36206	886.0882	835.3721	-50.7161

**Table 5** Calculated HOMO and LUMO energy, HOMO–LUMO energy gap ( $E_g$ ), adsorption energies of  $CS_2$  on the SiC nanotube surface ( $E_{ads}$ ) under the electric field of 0, 0.0025, 0.005 (a.u.) in parallel and perpendicular direction to the nanotube axis.

	Electric Field	$E_{HOMO}(eV)$	$E_{LUMO}(eV)$	$E_g(eV)$	$E_{ads}(Kj/mol)$
parallel direction	0	-4.16	-3.8461	0.31389	-163.98
	0.0025	-4.275	-3.9081	0.36693	2.93801
	0.005	-4.4282	-3.9269	0.5013	31.4774
perpendicular direction	0.0025	-4.2696	-3.9021	0.36747	-22.884
	0.005	-4.3191	-3.95	0.3691	-7.2838